Top Catal (2008) 51:146–157
DOI 10.1007/s11244-008-9127-7

ORIGINAL PAPER

Autothermal Reforming of Methane with Integrated CO_2 Capture in a Novel Fluidized Bed Membrane Reactor. Part 2 Comparison of Reactor Configurations

F. Gallucci · M. Van Sint Annaland · J. A. M. Kuipers

Published online: 24 October 2008

Abstract The reactor performance of two novel fluidized bed membrane reactor configurations for hydrogen production with integrated CO_2 capture by autothermal reforming of methane (experimentally investigated in Part 1) have been compared using a phenomenological reactor model over a wide range of operating conditions (temperature, pressure, H_2O/CH_4 ratio and membrane area). It was found that the methane combustion configuration (where part of the CH_4 is combusted in situ with pure O_2) largely outperforms the hydrogen combustion concept (oxidative sweeping combusting part of the permeated H_2) at low H_2O/CH_4 ratios (<2) due to in situ steam production, but gives a slightly lower hydrogen production rate at higher H_2O/CH_4 ratios due to dilution with combustion products. The CO selectivity was always much lower with the methane combustion configuration. Whether the methane combustion or hydrogen combustion configuration is preferred depends strongly on the economics associated with the H_2O/CH_4 ratio.

Keywords Membrane fluidized bed · Methane steam reforming · Autothermal reforming · Hydrogen · Membrane reactor

Nomenclature

Ai	Arrhenius pre-exponential factor (depends on reaction)
Ar	Archimedes number
A_T	Area of bed cross section (m^2)
$A^{membrane,n}$	Membrane surface area per cell n (m^2)
CSTR	Continuously stirred tank reactor
d_b	Bubble diameter (m)
$d_{b,avg}$	Average bubble diameter (m)
$d_{b,max}$	Maximum bubble diameter (m)
$d_{b,0}$	Initial bubble diameter (m)
d_p	Particle diameter (m)
D_g	Gas diffusity (m^2/s)
D_T	Bed diameter (m)
$E_{act,i}$	Activation energy for ith reaction (J/mol)
g	Gravitational acceleration (=9.81) (m/s^2)
h_{pc}	Heat transfer coefficient between a membrane and a gas–solid fluidized bed gas–solid fluidized bed (W/m^2 K)
h_f	Fluidized bed height (m)
h_{mf}	Minimum fluidized bed height (m)
$H_i^{T,x}$	Enthalpy of component i at temperature T at position x (J/mol)
$SF(Q)$	Heaviside function of Q
J_{H_2}	H_2 flux through membrane (mol/m^2 s)
k_g	Thermal conductivity gas mixture (W/m K)
k_i	Reaction rate constant for ith reaction (depends on Ai)
k_{Pd}	Membrane constant (mol/m s Pa^n)
K_{bc}	Volumetric interchange coefficient between bubble and cloud phase (s^{-1})
K_{be}	Volumetric interchange coefficient between bubble and emulsion phase (s^{-1})
K_{ce}	Volumetric interchange coefficient between cloud and emulsion phase (s^{-1})
$K_{be,i,n}$	Bubble-to-emulsion phase mass transfer coefficient for component I in cell n (s^{-1})
$K_{eq,i}$	Equilibrium constant for Ith reaction
L/S	Load to surface ratio ($m^3/(h\ m^2)$)
M_w[i]	Molar mass for component i (kg/mol)
N_b	Number of CSTRs in the bubble phase
N_e	Number of CSTRs in the emulsion phase

F. Gallucci · M. Van Sint Annaland (✉) · J. A. M. Kuipers
Fundamentals of Chemical Reaction Engineering Group, Faculty of Science and Technology, IMPACT, University of Twente, P.O. Box 217, 7500 AE Enschede, The Netherlands
e-mail: m.vansintannaland@tnw.utwente.nl

N_u	Nusselt number
n	Pressure exponent for Pd membrane
$n_{H_2,flux}$	H_2 flux (mol/s)
$n_{H_2,in}$	H_2 in (mol/s)
$n_{H_2,out}$	H_2 out (mol/s)
n_c	Number of components
n_{rxns}	Number of reactions
P	Reactor pressure (bar)
$P_{1,2}$	Product
p_i	Partial pressure for component i (atm)
$P_{m,Pd}$	Permeability of Pd membrane (mol/m s Pa^n)
$P_{m,Pd0}$	Pre-exponentional factor for permeability of Pd membrane (mol/m s Pa^n)
Q	Transfer term accounting for the change in volume
R	Gas constant (=8.3145) (J/mol K)
r_j	Reaction rate for jth reaction (mol/kg_{cat} s)
T_0	Wall temperature of the U-shaped membrane (K)
T_1	Inlet temperature U-shaped membrane (K)
$t_{m,Pd}$	Pd membrane thickness (m)
u_0	Superficial gas velocity at inlet (m/s)
$us_{L1,L2}$	Superficial gas velocity for phase L1 and cell L2 (m/s)
$u_{b,avg}$	Initial superficial bubble velocity (m/s)
u_{mf}	Minimum fluidization velocity (m/s)
u_{tot}	Velocity at bed inlet (m/s)
$v_{j,i}$	Stoichiometric coefficient for jth reaction and ith component
$V_{L1,L2}$	Volume for phase L1 and cell L2 (m^3)
$w_{L1,L2,L3}$	Weight fraction for phase L1, component L2 and cell L3
x	Fraction

Greek Variables

δ_b	Bubble phase fraction
δ_e	Emulsion phase fraction
ΔG_i	Gibb's free energy for ith reaction (J/mol)
$\Delta H_{i,ox}$	Heat of adsorption for ith component (J/mol)
ΔH_{298}	Heat of reaction at 298 K (J/mol)
ρ_g	Density of gas (kg/m^3)
ρ_p	Density of fluidized particles (kg/m^3)
ε_e	Emulsion phase porosity
ε_{mf}	Bed voidage at minimum fluidization velocity
μ_g	Viscosity of gas (Pa s)
χ	Amount of H_2 combustion
$\phi''^{membrane}_{i,mol}$	Molar flux component i through the membrane per cell (mol/m^2 s)
ϕ_m	Mass flow (kg/s)

Subscripts

0 Reactor inlet
b Bubble phase
e Emulsion phase
i Component *i*
j Number of reaction
n Number of CSTRs for emulsion of bubble phase

1 Introduction

Two novel fluidized bed membrane reactors for ultra-pure hydrogen production with integrated CO_2 capture by autothermal reforming of methane have been proposed in Part 1 of this work. In the methane combustion configuration, ultra-pure hydrogen is obtained via perm-selective Pd-based membranes, while part of the methane fed is oxidised in situ to generate the energy required for the methane steam reforming allowing for overall autothermal operation. Use of pure oxygen, avoids nitrogen dilution keeping the required reactor volume small and enables integration of CO_2 capture, but requires and expensive cryogenic distillation unit, which could be circumvented by integrating the O_2/N_2 separation inside the reactor by incorporating oxygen perm-selective (e.g. perovskite type) membranes. With experiments in a small pilot plant it has been demonstrated in Part 1 that autothermal methane reforming with in situ methane combustion can be carried out very efficiently (i.e. without any mass transfer limitations) in a fluidized bed membrane reactor without any problems associated with heat management. In the hydrogen combustion configuration, part of the permeated hydrogen is combusted to supply the energy for the methane steam reforming. In Part 1 the feasibility of the hydrogen combustion configuration has been experimentally tested and it has been shown that the permeated hydrogen can be combusted completely inside the Pd-membrane without additional catalyst and that the generated energy can be transferred back to the fluidized bed. Using oxidative sweeping on the permeate side of part of the perm-selective hydrogen membranes, CO_2 capture is integrated while use of oxygen perm-selective membranes in a high-temperature bottom section (required to achieve sufficiently high O_2 fluxes) in the methane combustion configuration is circumvented. For actual application of these oxygen perm-selective membranes, further development on the mechanical and chemical stability and sealing of these ceramic membranes is essential. However, the question remains whether the methane combustion configuration would be preferred, should the problems with oxygen perm-selective membranes be overcome. The objective of the second part of this work is to compare the reactor performance of the methane and hydrogen combustion configurations via a modelling study. First, the reactor model and the underlying assumptions are outlined,

which is subsequently validated by experiments presented in Part 1. Then, the model is used to compare the reactor performance in terms of methane conversion, product selectivity and hydrogen recovery and the effect of the operating conditions thereon.

2 Fluidized Bed Membrane Reactor Model

A frequently used phenomenological description of the two-phase flow phenomena in fluidized bed reactors is based on the bubble assemblage model, originally proposed by Kato and Wen [1]. In this one-dimensional model the fluidized bed is divided into a number of ideally-mixed reactors (CSTRs), with the same number of CSTRs for the bubble and emulsion phase where the size of the CSTR is related to the local bubble size. Based on this model, a one-dimensional two-phase model for a membrane-assisted fluidised bed reactor has been developed by Deshmukh et al. [2, 3]. Similar types of models have been used by the groups of Grace and Elnashaie and their co-workers [4–6]. In their model the number of CSTRs in the cascade and the sizes of the CSTRs are not directly related to the local bubbles size, but to the extent of gas back-mixing in each phase, which should be determined with independent experiments. A schematic representation of the gas flows between the compartments of the bubble and emulsion phases is depicted in Fig. 1. The model assumptions are as follows:

- The reactor consists of one (hydrogen combustion configuration) or two (methane combustion configuration) membrane-assisted fluidized bed sections.
- In each section dead-end and U-shaped (i.e. with sweep gas) hydrogen perm-selective membranes or oxygen perm-selective membranes can be integrated.
- Each section consists of two phases, viz. the bubble and emulsion phase.
- The gas flowing through the emulsion phase is considered to be completely mixed in each section and at incipient fluidization conditions.
- The bubble phase gas is assumed to be in plug flow (i.e. large number of CSTRs), where the bubble size and the bubble rise velocity changes for each section.
- The heterogeneous reactions (methane combustion, methane steam reforming and water–gas shift reactions) take place only in the emulsion phase, assuming that the bubble phase is free of catalyst particles. (Note that it has been experimentally verified that the contribution by homogeneous gas phase reactions can be neglected).
- Gas removed from the fluidised bed via membranes is assumed to be extracted from both the emulsion phase and bubble phase, distributed according to the local bubble fraction. The gas extracted from the emulsion phase is subsequently instantaneously replenished via exchange from the bubble phase (to maintain the emulsion phase at minimum fluidization conditions) (following [2, 3]).
- The bubble-to-emulsion phase mass transfer coefficients are assumed constant along the bed height for each section.
- A uniform temperature is assumed throughout an entire section of the fluidized bed, assuming no heat losses to the surroundings (adiabatic conditions) and no heat transfer limitations between the bubble and emulsion phase [7, 8].
- Related to the U-shaped hydrogen perm-selective membranes: it is assumed that all the permeated H_2 is combusted inside the membrane (provided that sufficient O_2 is available, as was demonstrated experimentally in Part 1), that the outlet temperature of the sweep gas is equal to the uniform temperature in the bed and that the temperature of the U-shaped membrane equals the bed temperature.

The overall (bubble and emulsion phase) component mass conservation equations have been formulated, accounting for chemical transformations in the emulsion phase and a net gas production due to the chemical reactions and gas withdrawal (hydrogen) and feeding (oxygen) via membranes (see Table 1, an explanation of the symbols used can be found in the nomenclature at the end of the paper). The overall energy balance equations have been listed in Table 2, accounting for possible energy exchange via the sweep gas. These equations are solved for each CSTR in each section of the membrane fluidized bed reactor. The degree of back-mixing is represented in terms of the number of CSTRs in series, where N_e stands for the number of CSTRs in the emulsion phase and N_b for the factor of additional CSTRs in the gas phase. If N_e equals 1, a completely back-mixed emulsion phase is represented.

Empirical correlations for the mass transfer coefficients and fluidization properties of the fluidized beds have been taken from [2, 3] and are summarized in Table 3. Although these correlations were originally obtained for beds without internals, it is assumed that the fluidized bed reactor with membranes can be reasonably well described with these equations. By means of simulations and experimental validation, Deshmukh and co-workers have shown that the axial gas phase back-mixing in the emulsion phase is strongly reduced because of the presence of and permeation through the membranes. Typically, insertion of the membranes enhances bubble break-up, resulting in improved bubble-to-emulsion phase mass transfer [2, 3].

The kinetic rate expressions for methane combustion, methane steam reforming and water–gas shift, summarised

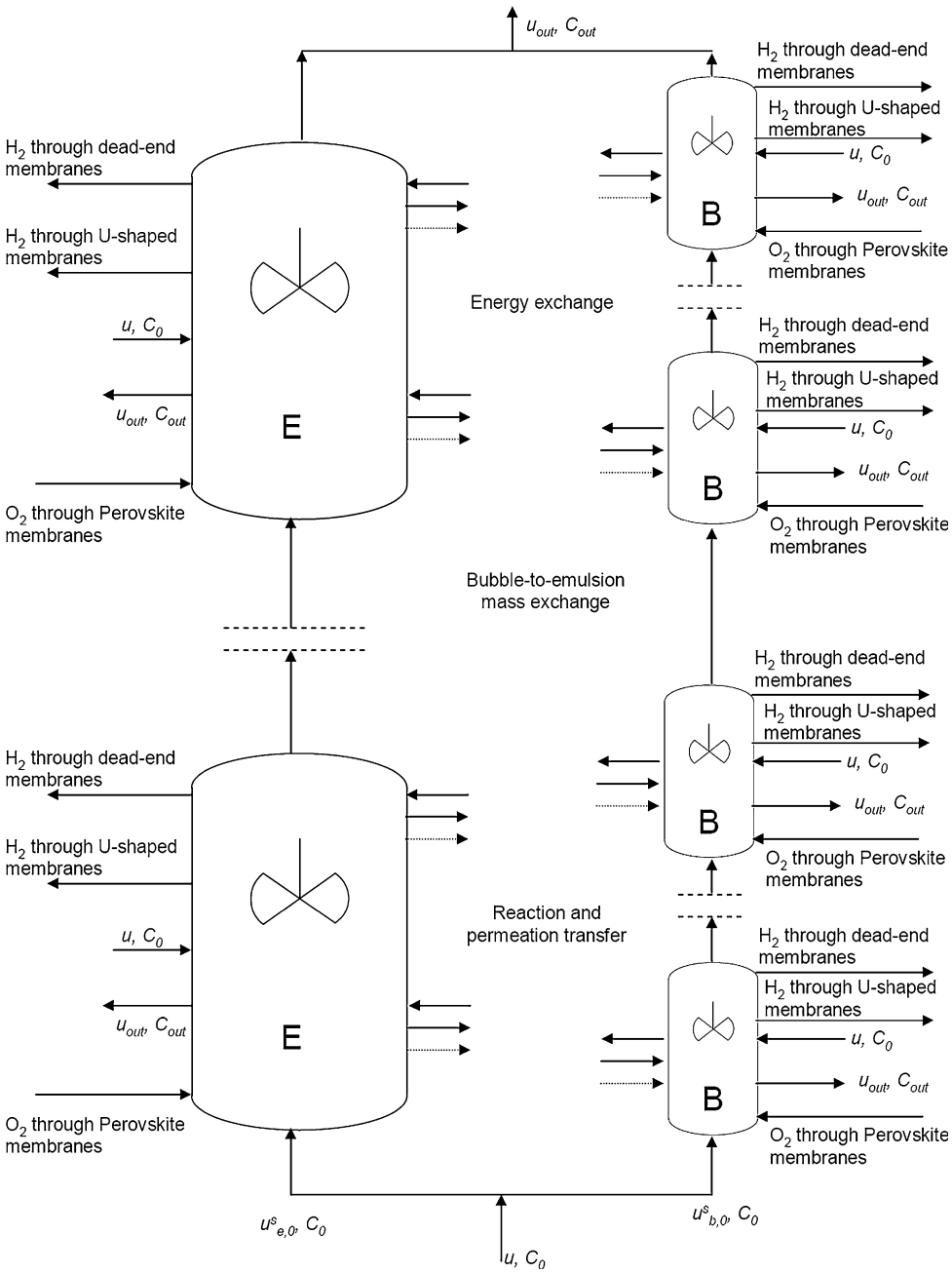

Fig. 1 A schematic representation of the 2-phase fluidized bed reactor model (FBMR)

in Table 4, are taken from [9, 10]. Although these kinetic rate expressions were developed for a different catalyst system, their use is justified h.l. since no kinetic limitations were observed (see Part 1). Selective removal of H_2 using Pd-based membranes has been modelled with a Sievert's type flux expression, using experimental data from [11] and experimental data reported in Part 1 (see Table 4). Pure component physical data have been taken from [12], while mixture properties have been computed following Reid et al. [13].

The overall feed ratios of CH_4, H_2O and O_2 to obtain overall autothermal operation for both reactor configurations can be easily determined by combining the methane steam reforming + water–gas-shift reaction (1), with methane combustion (2) and/or hydrogen combustion (3):

Methane steam reforming + water--gas-shift: $CH_4 + 2H_2O \Leftrightarrow CO_2 + 4H_2$ (1)

Methane combustion: $\delta^*(CH_4 + 2O_2 \Leftrightarrow CO_2 + 2H_2O)$ (2)

Hydrogen combustion: $\chi^*(H_2 + {}^1/_2O_2 \Leftrightarrow H_2O)$ (3)

The overall reaction can thus be represented by

Table 1 Mass balance equations for each CSTR in each section of the fluidized membrane reactor (Reprinted from 'Fluidised bed membrane reactor for ultrapure hydrogen production via methane steam reforming: Experimental demonstration and model validation', Chem. Eng. Sci., 62, 2989–3007 (2007), with permission from Elsevier)

Total mass balance

$$u^s_{b,n-1}A_T\rho_{b,n-1} - u^s_{b,n}A_T\rho_{b,n} + u^s_{e,n-1}A_T\rho_{e,n-1} - u^s_{e,n}A_T\rho_{e,n} + \sum_{i=1}^{n_c}\left\{\phi''^{membrane}_{i,mol}M_{w,i}A_{membrane}e_{b,n} + \phi''^{membrane}_{i,mol}M_{w,i}A_{membrane}\left(1-e_{b,n}\right)\right\} = 0$$

Bubble phase component mass balances[a]

$$u^s_{b,n-1}A_T\rho_{b,n-1} - u^s_{b,n}A_T\rho_{b,n} - \sum_{i=1}^{n_c}K_{be,i,n}V_{b,n}\rho_{b,n}\left(w_{b,i,n}-w_{e,i,n}\right) + \sum_{i=1}^{n_c}\phi''^{membrane}_{i,mol}M_{w,i}A_{membrane}e_{b,n} + \left[w_{e,i,n}SF(Q) - w_{b,i,n}SF(-Q)\right] = 0$$

Emulsion phase component mass balances[a]

$$u^s_{e,n-1}A_T\rho_{e,n-1} - u^s_{e,n}A_T\rho_{e,n} - \sum_{i=1}^{n_c}K_{be,i,n}V_{b,n}\rho_{b,n}\left(w_{b,i,n}-w_{e,i,n}\right) - \sum_{i=1}^{n_c}\phi''^{membrane}_{i,mol}M_{w,i}A_{membrane}\left(1-e_{b,n}\right) - \left(\sum_{j=1}^{n_{rxn}}v_{j,i}r_j\right)V_{e,n}\rho_{p,n}(1-e_e) - \left[w_{e,i,n}SF(Q) - w_{b,i,n}SF(-Q)\right] = 0$$

Transfer term

$$Q = u^s_{e,n-1}A_T\rho_{e,n-1} - u^s_{e,n}A_T\rho_{e,n} \pm \sum_{i=1}^{n_c}\phi''^{membrane}_{i,mol}A_{membrane}\left(1-e_{b,n}\right) + \sum_{i=1}^{n_c}K_{be,i,n}V_{b,n}\rho_{b,n}\left(w_{b,i,n}-w_{e,i,n}\right)$$

$$u^s_{e,n}A_T = u_{e,n}A_T\left(1-e_{b,n}\right)$$

where $u^s_{b,0}A_T = u_{tot}A_Te_{b,0}$

$$u^s_{e,0}A_T = u_{tot}A_T\left(1-e_{b,0}\right)$$

[a]Note that $SF(x) = \begin{cases} x \text{ if } x > 0 \\ 0 \text{ if } x \le 0 \end{cases}$

Table 2 Energy balance equations for each CSTR in each section of the fluidized membrane reactor

Energy balance (both concepts)

$$\left\{\sum_{i=1}^{n_c}H_i^{T_{feed}}\left(u^s_{b,n=0}A_T\rho_{b,i,n=0} + u^s_{e,n=0}A_T\rho_{e,i,n=0}\right) - \sum_{i=1}^{n_c}H_i^{T_{out}}\left(u^s_{b,n=N}A_T\rho_{b,i,n=N} + u^s_{e,n=N}A_T\rho_{e,i,n=N}\right)\right\} \pm \left\{\sum_{i=1}^{n_c}H_i^{T_{out}}\left(\phi''^{membrane}_{i,mole}M_{w,i}A_Te_{b,n} + \phi''^{membrane}_{i,mole}M_{w,i}A_T\left(1-e_{b,n}\right)\right)\right\} + E = 0$$

In situ air preheating (concept 1)

Top section

$$E = \left\{\sum_{i=1}^{n_c}H_i^{T_{air}}\phi_{i,mole,in}M_{w,i} - \sum_{i=1}^{n_c}H_i^{T_{bottom}}\phi_{i,mole,out}M_{w,i}\right\} + \left\{\sum_{i=1}^{n_c}H_i^{T_{bottom}}\phi_{i,mole,in}M_{w,i} - \sum_{i=1}^{n_c}H_i^{T_{top}}\phi_{i,mole,out}M_{w,i}\right\}$$

Bottom section

$$E = \left\{\sum_{i=1}^{n_c}H_i^{T_{bottom}}\phi_{i,mole,in}M_{w,i} - \sum_{i=1}^{n_c}H_i^{T_{top}}\phi_{i,mole,out}M_{w,i}\right\}$$

H_2 *combustion in the U shape membrane (concept 2)*

$$E = \left\{\sum_{i=1}^{n_c}H_i^{T_{feedU}}\phi_{i,mole,in}M_{w,i} - \sum_{i=1}^{n_c}H_i^{T_{top}}\phi_{i,mole,out}M_{w,i}\right\}$$

Table 3 Empirical correlations for the mass transfer coefficients and fluidization properties (Reprinted from 'Development of a Membrane-Assisted Fluidized Bed Reactor. 2 Experimental Demonstration and Modeling for the Partial Oxidation of Methanol', Ind. Eng. Chem. Res., 44 (16), 5966–5976, 2005, with permission from American Chemical Society)

Parameter	Equation
Archimedes Number	$Ar = \frac{d_p^3 \rho_g (\rho_p - \rho_g) g}{\mu_g^2}$
Minimum fluidization velocity	$u_{mf} = \left(\frac{\mu_g}{\rho_g d_p}\right)\left(\sqrt{(27.2)^2 + 0.0408Ar} - 27.2\right)$
Bed voidage at minimum fluidization velocity	$\varepsilon_{mf} = 0.586 Ar^{-0.029}\left(\frac{\rho_g}{\rho_p}\right)^{0.021}$
Projected tube area for a square bed	$A_T = {D_T}^2$
Rise velocity of a single bubble	$u_{br} = 0.711(g d_b)^{\frac{1}{2}}$
Velocity of rise of swarm of bubbles	$u_b = u_0 - u_{mf} + 0.711(g d_b)^{\frac{1}{2}}$
Initial bubble diameter (Porous plate distributor)	$d_{b0} = 0.376(u_0 - u_{mf})^2$
Maximum bubble diameter	$d_{b,\max} = D_T$
Superficial bubble gas velocity	$\frac{u^s_{b,\max} - u^s_b}{u^s_{b,\max} - u^s_{b,0}} = \exp\left(\frac{0.55z}{h_{mf} D_T}\right)$
Maximum superficial bubble gas velocity	$u^s_{b,\max} = u_0 - u_{mf}$
Initial superficial bubble gas velocity	$u^s_{b,0} = u_{br,0}\delta_{b0}$ where $\delta_{b0} = \left(1 - \frac{h_{mf}}{h_f}\right)$
Superficial emulsion gas velocity	$u^s_e = u_0 - u^s_b$
Bubble phase fraction	$\delta_b = \frac{u^s_b}{u_b}$
Emulsion phase fraction	$\delta_{en} = 1 - \delta_{bn}$
Volume of emulsion phase in the nth compartment	$V_{e,n} = A_T \frac{h_f}{N_b}$
Volume of bubble in the nth compartment	$V_{b,n} = A_T \frac{h_f}{N_b}\delta_{b,n}$
Bubble diameter	$d_b = d_{b,\max} - (d_{b,\max} - d_{b,0}) e^{\left(\frac{-0.3z}{D_T}\right)}$
Height of bed expansion	$h_f = h_{mf}\frac{C_1}{C_1 - C_2}$ where, $C_1 = 1 - \frac{u_{b,0}}{u_{b,avg}}\exp\left(-\frac{0.275}{D_T}\right)$ $C_2 = \frac{u^s_b}{u_{b,avg}}\left[1 - \exp\left(-\frac{0.275}{D_T}\right)\right]$
Average bubble rise velocity	$u_{b,avg} = u_0 - u_{mf} + 0.711(g d_{b,avg})^{\frac{1}{2}}$
Gas exchange coefficient	$K_{bc} = 4.5\left(\frac{u_{mf}}{d_p}\right) + 5.85\left(\frac{D_g^{\frac{1}{2}} g^{\frac{1}{4}}}{d_b^{\frac{5}{4}}}\right)$ $K_{ce} = 6.77\left(\frac{D_g \varepsilon_{mf} u_b}{d_b^3}\right)^{\frac{1}{2}}$ $\frac{1}{K_{be}} = \frac{1}{K_{bc}} + \frac{1}{K_{ce}}$

$$CH_4 + \frac{(2\delta + \frac{1}{2}\chi)}{(1+\delta)}O_2 + \frac{(2 - 2\delta - \chi)}{(1+\delta)}H_2O \Leftrightarrow CO_2 + \frac{(4-\chi)}{(1+\delta)}H_2 \quad (4)$$

which can be further rearranged into

$$CH_4 + \xi O_2 + 2(1-\xi)H_2O \Leftrightarrow CO_2 + 2(2-\xi)H_2 \quad (5)$$

with

$$\xi = \frac{(2\delta + \frac{1}{2}\chi)}{(1+\delta)}.$$

The amount of methane or hydrogen that needs to be combusted to achieve autothermal conditions relative to the amount of methane reformed and shifted then follows easily from:

Methane combustion configuration:

Table 4 The kinetic rate expressions used in the model

Reactions	Stoichiometry and reaction rate equations
1. Methane combustion on Pt catalyst [9]	$CH_4 + 2O_2 \Leftrightarrow CO_2 + 2H_2O$ $r_1 = \frac{k_{1a}\left(p_{CH_4}p_{O_2}\right)}{\left(1+K^{OX}_{CH_4}p_{CH_4}+K^{OX}_{O_2}p_{O_2}\right)^2} + \frac{k_{1b}\left(p_{CH_4}p_{O_2}\right)}{\left(1+K^{OX}_{CH_4}p_{CH_4}+K^{OX}_{O_2}p_{O_2}\right)}$
2. Methane steam reforming on Ni catalyst [10]	$CH_4 + H_2O \Leftrightarrow CO + 3H_2$ $r_1 = \frac{k_1\left(p_{CH_4}p_{H_2O} - p^3_{H_2}p_{CO}/K_{eq,1}\right)}{p^{1.596}_{H_2O}}$
3. Water–gas shift on Ni catalyst [10]	$CO + H_2O \Leftrightarrow CO_2 + H_2$ $r_2 = \frac{k_2\left(p_{CO}p_{H_2O} - p_{H_2}p_{CO_2}/K_{eq,2}\right)}{p_{H_2O}}$

where $k_i = A_i \exp\left(\frac{-E_{act,i}}{RT}\right)$, $K_i^{OX} = A_i^{OX} \exp\left(\frac{-\Delta H_i^{OX}}{RT}\right)$, $K_{eq,i} = \exp\left(\frac{-\Delta G_i}{RT}\right)$

Arrenius parameters, equilibrium constants for SRM and WGS and van't Hoff parameters for methane combustion [15]

Constant	Value	Units	Constant	Value	Units
A_{1a}	8.11×10^5	mol/(bar^2 k_{cat} s)	$E_{act,1a}$	86×10^3	J/mol
A_{1b}	6.82×10^2	mol/(bar^2 k_{cat} s)	$E_{act,1b}$	86×10^3	J/mol
A_1	2.62×10^5	mol/(bar$^{0.404}$ k_{cat} s)	$E_{act,1}$	106.9×10^3	J/mol
A_2	2.45×10^2	mol/(bar k_{cat} s)	$E_{act,2}$	54.5×10^3	J/mol
$A^{OX}_{CH_4}$	1.26×10^{-1}	bar^{-1}	$\Delta H^{OX}_{CH_4}$	-27.3×10^3	J/mol
$A^{OX}_{O_2}$	7.87×10^{-7}	mol/(bar^2 k_{cat} s)	$\Delta H^{OX}_{O_2}$	-92.8×10^3	J/mol

Flux of H_2 through Pd membranes

$J_{H_2} = \frac{P_{m,Pd}}{t_{m,Pd}}\left(p^n_{H_2,f} - p^n_{H_2,p}\right)$ where

$Ln\left(P_{m,Pd}\right) = a_1 \times T^2 + a_2 \times T + a_3$

$n = b_1 \times T^2 + b_2 \times T + b_3$

$a_1 = 5.18253 \times 10^{-5} a_2 = -6.47388 \times 10^{-2} a_3 = -7.23505$

$b_1 = -3.90979 \times 10^{-6} b_2 = 4.96376 \times 10^{-3} b_3 = -0.569705$

$t_{m,Pd}$ = membranethickness $= 4.5 \times 10^{-6}$[m]

T = temperature[K]

$$\chi = 0 \quad \Rightarrow \quad \delta = \frac{\xi}{(2-\xi)}$$

Hydrogen combustion configuration:

$$\delta = 0 \quad \Rightarrow \quad \chi = 2\xi$$

The relative amount of O_2 and steam required for autothermal conditions can be determined with the following equation:

$$\sum_{i=1}^{nc} v_i^{\xi} * H_i^T = 0 \tag{6}$$

where v_i^{ξ} is the stoichiometric coefficient of component i for a selected composition H_i^T is the enthalpy of component i for a selected temperature (J/mol)

For a selected temperature, Eq. 6 can be solved for ξ using reaction Eq. 5, and consequently δ (CH_4 combustion configuration) or χ (H_2 combustion configuration) can be calculated. The overall O_2/CH_4 and H_2O/CH_4 ratios as function of the temperature to attain autothermal operation are given in Fig. 2. For example, it can be seen that for a reactor temperature of 600 °C, the overall O_2/CH_4 and H_2O/CH_4 ratios are approximately 0.379 and 1.242, respectively, which results in an overall production of 3.242 mol H_2 and 1 mol CO_2 per mol CH_4. Note that from an overall energetic viewpoint, the methane combustion and hydrogen combustion configurations are identical and that the same maximal H_2 yield can be achieved, provided that complete CH_4 and CO conversion can be realized. The described reactor model is subsequently used to compare the actual reactor performance as a function of the operating conditions in terms of the following parameters:

$$\text{Methane conversion} = \frac{\phi_{CH_4,in} - \phi_{CH_4,out}}{\phi_{CH_4,in}}$$

$$\text{Hydrogen recovery} = \frac{\phi_{H_2,\text{extracted via dead-end membranes}}}{\phi_{H_2,\text{produced}}}$$

$$\text{Hydrogen burned} = \frac{\phi_{H_2,\text{extracted via U-shaped membranes}}}{\phi_{H_2,\text{produced}}}$$

$$\text{Hydrogen in the exhaust} = \frac{\phi_{H_2,out}}{\phi_{H_2,\text{produced}}}$$

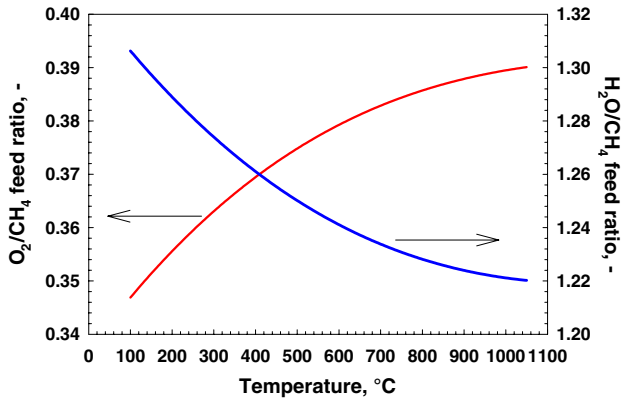

Fig. 2 Overall feed ratios as a function of temperature to attain autothermal operation

$$\text{CO selectivity} = \frac{\phi_{CO,out}}{\phi_{CO,out} + \phi_{CO_2,out}}$$

$$\text{CO}_2\text{ selectivity} = \frac{\phi_{CO_2,out}}{\phi_{CO,out} + \phi_{CO_2,out}}$$

3 Model Validation

The fluidized bed membrane reactor model has already been validated for the methane combustion configuration in a previous work [11]. Here, model predictions are compared with experimental data [14] for the hydrogen combustion concept with hydrogen production via the dead-end membranes and energy supply via oxidative sweeping in the U-shaped membranes. For a selected case, the effect of the degree of gas back-mixing in the bubble and emulsion phases has been investigated and the results are summarised in Table 5. The CH_4 conversion slightly increases when increasing the number of CSTRs for the bubble phase, while assuming the emulsion phase perfectly mixed. The reason is not the decreased degree of axial back-mixing in the bubble phase, but is related to a better representation of the change in bubble size along the bed height. For higher N_b, the presence of smaller bubbles at the bottom of the bed is accounted for enhancing the mass transfer, resulting in increased CH_4 conversion [11]. As can be discerned from Table 5, even when assuming an infinite number of CSTRs in the bubble phase, the model underpredicts the experimentally determined CH_4 conversion. The discrepancy is related to the extent of gas back-mixing in the emulsion phase. Fixing the ratio of the number of bubble phase CSTRs to the number of emulsion phase CSTRs (N_b = 3), the degree of back-mixing in the emulsion phase has been reduced (N_e increased), which resulted in a strong increase in the membrane flux through both types of membranes and corresponding increase in the CH_4 conversion. It can be concluded that for $N_e > 6$, the predicted fluxes match reasonably well with the measured fluxes, indicating that the membrane reactor can be best described by assuming both the bubble and emulsion phases in plug flow. Due to the presence of and permeation through the membranes the fluidized bed membrane reactor approaches the Holy Grail of chemical reaction engineers: the isothermal plug flow reactor. With simulations it has been confirmed that for the conditions investigated (low relative superficial gas velocities in combination with a relatively large gas extraction via the membranes) bubble-to-emulsion phase limitations and kinetic limitations are negligible. Finally, model predictions (assuming N_e = 6 and N_b = 3) have been compared with experimental data for two different H_2O/CH_4 ratios (see Table 6), showing that the reactor model predicts the measured data reasonably well.

Table 5 Comparison between experimental data and MAFB model prediction. (Hydrogen combustion configuration, T = 500 °C, p = 3 bar, N_2/CH_4 = 2, H_2O/CH_4 = 4 u/u_{mf} = 2)

Measured data				
CH_4 conversion, %	68.4			
CO selectivity, %	6.4			
H_2 flow dead-end, NmL/min	529.83			
H_2 flow U-shaped membrane, NmL/min	129.85			
Total H_2 flow/Total H_2 production	74.39			
MAFB model prediction				
N_b	1	3	5	10
Degree of back-mixing in bubble phase N_e = 1 and N_b = variable				
CH_4 conversion, %	66.16	66.53	66.53	66.53
CO selectivity, %	7.13	7.15	7.15	7.15
H_2 flow dead-end, NmL/min	471.18	472.45	472.47	472.47
H_2 flow U-shaped membrane, NmL/min	105.29	105.58	105.58	105.58
Total H_2 flow/Total H_2 production	72.25	72.11	72.11	72.11
Degree of back-mixing in emulsion phase N_b = 3 and N_e = variable				
CH_4 conversion, %	66.53	68.65	69.13	69.29
CO selectivity, %	7.15	6.81	6.77	6.76
H_2 flow dead-end, NmL/min	472.45	504.89	513.73	516.69
H_2 flow U-shaped membrane, NmL/min	105.58	112.83	114.80	115.46
Total H_2 flow/Total H_2 production	72.11	73.90	74.44	74.69

4 Comparison of Reactor Configurations

The CH_4 conversion, CO selectivity and total H_2 production rate at overall autothermal conditions have been compared for the two reactor configurations as a function

Table 6 Comparison between experimental data and model predictions. (Hydrogen combustion configuration, $T = 500$ °C, $p = 3$ bar, $N_2/CH_4 = 2$, $u/u_{mf} = 2$, $N_e = 6$, $N_b = 3$)

	Measured data		MAFB model	
H_2O/CH_4 ratio	3	4	3	4
CH_4 conversion, %	57.92	68.36	59.86	69.13
CO selectivity, %	8.21	6.47	7.89	6.77
H_2 production, NmL/min	869.39	886.77	860.96	844.34
H_2 flow dead-end, NmL/min	525.96	529.83	533.12	513.73
H_2 flow U-shaped membrane, NmL/min	125.86	129.85	119.14	114.80
Total H_2 flow/total H_2 production	74.97	74.39	75.76	74.44

of the load-to-surface ratio (L/S), defined as the volumetric methane feed flow rate divided by the total Pd membrane area, for different temperatures in the (top section of the) fluidized bed (see Table 7). With appropriate load-to-surface ratios virtually complete CH_4 conversion and comparable H_2 production rates can be achieved, however, the CO selectivity is always much lower with the methane combustion concept for all temperatures investigated. This difference is related to the fact that in the methane combustion concept, part of the CH_4 is converted in situ into CO_2 and H_2O (in a bottom section) and that the additional steam thus produced helps shifting the reforming and water–gas-shift equilibria, while in the hydrogen combustion configuration the steam is produced inside the U-shaped Pd membranes and thus not available to shift the reactions towards the desired products. At an overall feed ratio of H_2O/CH_4 of 1.75, the H_2O/CH_4 in the top section of the methane combustion configuration actually amounts to 5, which explains the much lower CO selectivity with this configuration. For low H_2O/CH_4 molar feed ratios, the hydrogen production rate is much higher with the methane combustion configuration (see Fig. 3), but at higher

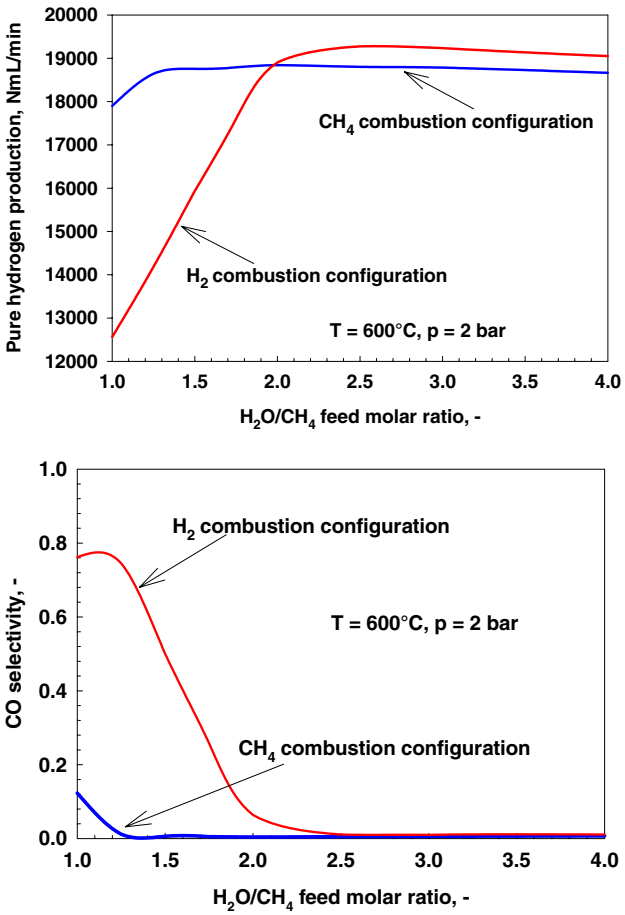

Fig. 3 Pure hydrogen production and CO selectivity versus H_2O/CH_4 feed molar ratio

H_2O/CH_4 molar feed ratios, the hydrogen production rate of the hydrogen combustion configuration strongly increases and at H_2O/CH_4 ratios above 2, the hydrogen combustion configuration even slightly outperforms the methane combustion configuration. At these higher H_2O/CH_4 ratios the adverse dilution effect via direct oxygen

Table 7 CH_4 conversion, H_2 production and exhaust gas selectivities as a function of the (top section) temperature for the methane and hydrogen combustion configurations ($P = 20$ bar, $u/u_{mf} = 3$, $O_2/CH_4 = 0.39$)

T (°C)	Methane combustion configuration			Hydrogen combustion configuration		
	L/S $m^3/h\ m^2$	Pure H_2 NmL/min	Bottom T°C	L/S $m^3/h\ m^2$	Pure H_2 NmL/min	Comb H_2 NmL/min
550	0.42	18332	1127	0.42	17788	4620
600	0.42	18779	1174	0.42	18950	4640
650	0.42	18872	1212	0.42	19262	4610
700	0.42	18965	1189	0.42	19362	4613
	CH_4 conversion	CO selectivity	CO_2 selectivity	CH_4 conversion	CO selectivity	CO_2 selectivity
550	0.99	0.02	0.98	0.98	0.13	0.87
600	1	0.003	0.997	1	0.06	0.94
650	1	0.0002	0.9998	1	0.02	0.98
700	1	5.37×10^{-6}	0.999995	1	0.002	0.998

Table 8 Hydrogen production, methane conversion and CO selectivity for the methane combustion configuration using air or pure oxygen ($T = 650$ °C, $p = 2$ bar, $H_2O/CH_4 = 2.48$, $u/u_{mf} = 3$, $O_2/CH_4 = 0.41$)

O_2 or air	L/S $m^3/h\ m^2$	CH_4 conversion	CO selectivity	Pure H_2 production	Pure H_2 recovery
Air	0.42	0.99999925	0.0030	18908.67	99.85
O_2	0.58	0.99999875	0.0030	18910.65	99.85
O_2	0.42	1	0.0003	18951.64	99.99

addition outweighs the benefits of shifting the reaction equilibria by the additional steam production.

In the calculations for the methane combustion concept it has been assumed that pure oxygen either directly via the feed or via oxygen perm-selective membranes has been fed to the reaction mixture, which avoids a costly downstream CO_2/N_2 separation, but also avoids dilution of the reaction mixture with N_2, which would result in lower hydrogen partial pressures and hydrogen permeation fluxes. This effect has been quantified by performing simulations using air instead of N_2, summarized in Table 8. For a typical case (top section at 650 °C and 2 bar with a H_2O/CH_4 feed ratio of 2.48), the required membrane area increases with 27% (i.e. lower load-to-surface area) to achieve a similar reactor performance, in terms of H_2 production rate, H_2 recovery, CO selectivity and CH_4 conversion, when using air instead of pure oxygen.

In Fig. 4 the required membrane area to obtain complete methane conversion at a fixed CO selectivity of 0.02 is shown as a function of the operating pressure and temperature for the hydrogen combustion configuration. An increase in the reactor pressure has a twofold effect on the reactor performance: a higher pressure negatively affects the steam reforming reaction equilibrium, but increases the driving force for hydrogen permeation through the membranes. From the figure it is clear that the second effect dominates and the required membrane area strongly decreases when increasing the reactor pressure up to about 10 bar, after which the effect of the pressure levels off. An increase in the temperature strongly decreases the required membrane area due to its positive effect on the endothermic steam reforming equilibrium and the strong increase in hydrogen permeance through the membranes. The operating temperature is currently, however, limited to about 700 °C for Pd-based membranes in view of membrane stability/life time. For the methane combustion configuration quite similar effects have been found and are not shown in this paper.

The required membrane area to achieve (virtually) complete CH_4 conversion and a target CO selectivity (and hence H_2 recovery) is shown in Fig. 5 for the hydrogen combustion configuration (at 750 °C and 20 bar). The required membrane area increases with only 33% to reduce the CO selectivity tenfold from 0.02 to 0.002. However, to further decrease the CO selectivity, the required membrane area strongly increases, especially at lower operating temperatures (see Table 9). To decrease the CO selectivity from 0.02 to 5×10^{-5} the required membrane area increases with 120% at 750 °C, while at 650 °C the required membrane area increases 10-fold! For the methane combustion configuration similar results were found, but the CO selectivity is already much lower due to the in situ steam generation.

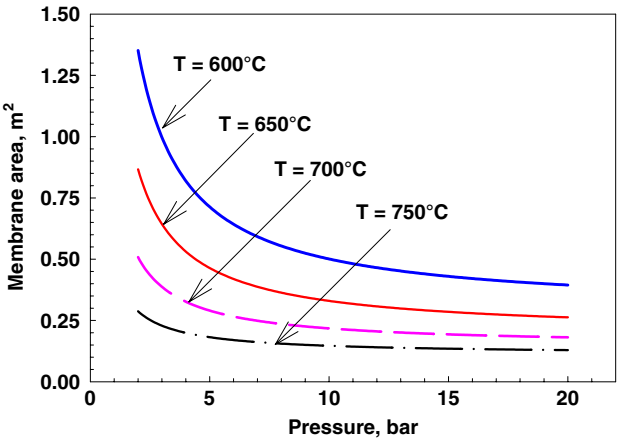

Fig. 4 Membrane area as a function of pressure and versus temperature. (Hydrogen combustion configuration, Methane conversion = 1, CO selectivity = 0.02)

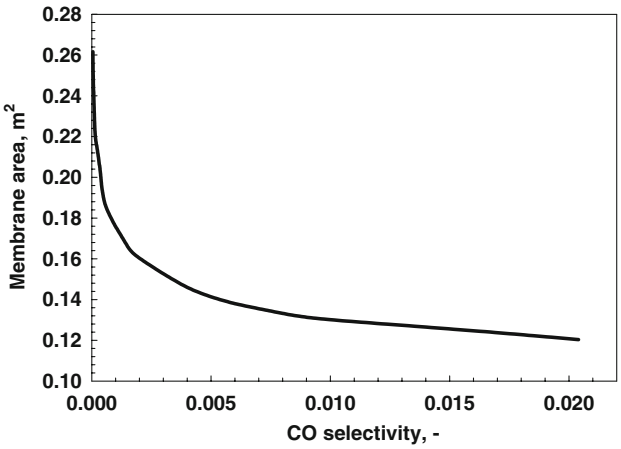

Fig. 5 Membrane area versus CO selectivity. (Hydrogen combustion configuration, CH_4 conversion = 1, $T = 750$ °C, $P = 20$ bar)

Table 9 Membrane area versus the CO selectivity for different temperatures. (Hydrogen combustion configuration, CH_4 conversion = 1, P = 20 bar, H_2O/CH_4 = 2, u/u_{mf} = 3, O_2/CH_4 = 0.39)

Temperature	CO selectivity	Membrane area m^2
650	0.02	0.238
700	0.02	0.165
750	0.02	0.120
650	0.00005	2.362
700	0.00005	0.696
750	0.00005	0.262

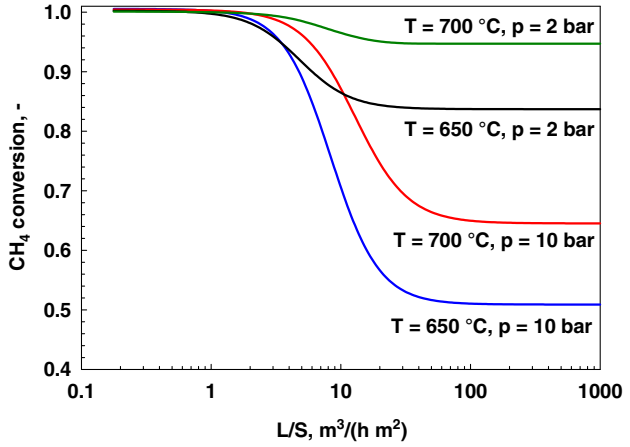

Fig. 6 CH_4 conversion versus L/S. (Methane combustion configuration, different pressures and temperatures H_2O/CH_4 = 2)

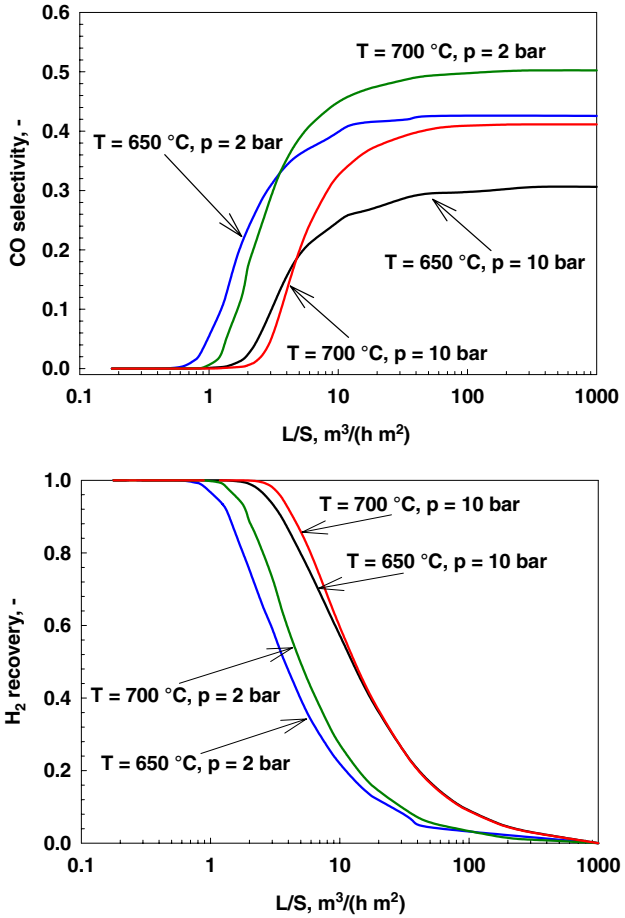

Fig. 7 CO selectivity and H_2 recovery versus L/S. (Methane combustion configuration, different pressures and temperatures H_2O/CH_4 = 2)

Finally, the reactor performance in terms of CH_4 conversion, CO selectivity and H_2 recovery is plotted as a function of the load-to-surface ratio (reciprocal to the required membrane area) in Figs. 6 and 7 for different temperatures and pressures for the methane combustion configuration. Figure 6 clearly shows that for each temperature and pressure investigated, complete CH_4 conversion can be achieved with a load-to-surface ratio below 1, while with a load-to-surface ratio above 100 the equilibrium CH_4 conversion is obtained and the extent of hydrogen extraction via the membranes is too small to affect the steam reforming equilibrium. With a load-to-surface ratio below 0.6 complete CH_4 conversion, maximal H_2 recovery and minimal CO selectivity can be realized. However, a good compromise between reactor performance and membrane investment costs is probably achieved with a load-to-surface ratio of 1–6, with which about 80% H_2 recovery and over 90% CH_4 conversion is obtained. However, for this case the CO selectivity might easily exceed 20%, so that a post-treatment of the retentate might be necessary. Alternatively, higher H_2O/CH_4 ratios could be used. For the hydrogen combustion configuration the same trends as presented in Figs. 6 and 7 are found with the exception of a much higher CO selectivity than with the methane combustion configuration.

5 Conclusions

The reactor performance (CH_4 conversion, CO selectivity, H_2 production rate) of two reactor concepts for autothermal reforming of methane with integrated CO_2 capture has been compared with a phenomenological reactor model, which was validated with experimental data. The required load-to-surface ratios (reciprocal to membrane area) have been determined at different operating conditions (pressure, temperature and H_2O/CH_4 ratios). It was found that with low H_2O/CH_4 ratios (<2) the methane combustion concept (with pure oxygen, either fed directly or via oxygen perm-selective membranes) largely outperforms the hydrogen combustion concept (with oxidative sweeping), due to the in situ steam production. However, at higher H_2O/CH_4 ratios the hydrogen production is slightly higher with the hydrogen combustion configuration, since it

avoids dilution with combustion products. At the H_2O/CH_4 ratio required for overall autothermal operation (1.24) higher CH_4 conversions and much lower CO selectivities can be realized with the methane combustion configuration. However, whether the methane combustion or hydrogen combustion configuration is preferred depends strongly on the economics associated with the H_2O/CH_4 ratio, i.e. the costs for steam production/availability of (high pressure) steam and the catalyst requirements to avoid carbonaceous deposits. In addition, for the methane combustion configuration an additional costly high-temperature bottom section with oxygen perm-selective membranes is required.

Acknowledgements The authors are grateful to the Dutch Ministry of Economic affairs for financial support of this work in the EOS program (project EOSLT05010).

References

1. Kato K, Wen C (1969) Bubble assemblage model for fluidized bed catalytic reactors. Chem Eng Sci 24:1351–1369
2. Deshmukh SARK, Laverman JA, Cents AHG, Van Sint Annaland M, Kuipers JAM (2005) Development of a membrane assisted fluidized bed reactor. 1. Gas phase back-mixing and bubble-to-emulsion phase mass transfer using tracer injection and ultrasound experiments. Ind Eng Chem Res 44:5955–5965
3. Deshmukh SARK, Laverman JA, Van Sint Annaland M, Kuipers JAM (2005) Development of a membrane assisted fluidized bed reactor. 2. Experimental demonstration and modeling for the partial oxidation of methanol. Ind Eng Chem Res 44:5966–5976
4. Constantineau JP, Grace JR, Lim CJ, Richards GG (2007) Generalized bubbling–slugging fluidized bed reactor model. Chem Eng Sci 62:70–81
5. Al-Sherehy F, Grace JR, Adris AM (2005) The influence of distributed reactant injection along the height of a fluidized bed reactor. Chem Eng Sci 60:7121–7130
6. Adris AM, Elnashaie SSEH, Hughes R (1991) Fluidized bed membrane reactor for the steam reforming of methane. Can J Chem Eng 69(5):1061–1070
7. Deshmukh SARK, Van Sint Annaland M, Kuipers JAM (2005) Heat transfer in a membrane assisted fluidised bed with immersed horizontal tubes. Int J Chem React Eng 3:A1
8. Patil CS, Van Sint Annaland M, Kuipers JAM (2006) Experimental study of a membrane assisted fluidized bed reactor for H_2 production by steam reforming of CH_4. Chem Eng Res Des 84:399–404
9. Trimm DL, Lam C-W (1980) Combustion of methane on platinum-alumina fibre catalysts-2. Design and testing of a convective-diffusive type catalytic combustor. Chem Eng Sci 35(8):1731–1739
10. Numaguchi T, Kikuchi K (1988) Intrinsic kinetics and design simulation in a complex reaction network: steam reforming. Chem Eng Sci 43:2295–2301
11. Patil CS, van Sint Annaland M, Kuipers JAM (2007) Fluidised bed membrane reactor for ultrapure hydrogen production via methane steam reforming: Experimental demonstration and model validation. Chem Eng Sci 62(11):2989–3007
12. Daubert TE, Danner RP (1998) Physical and thermodynamic properties of pure chemicals, Core Edition. Taylor & Francis, London
13. Reid RC, Prausnitz JM, Poling BE (1988) The properties of gases and liquids. McGraw-Hill Book Company, New York
14. Gallucci F, van Sint Annaland M, Kuipers JAM (submitted) Autothermal steam reforming of methane in a novel fluidized membrane reactor. Part 1 experimental demonstration. Top Catal
15. De Smet CRH, De Croon MHJM, Berger RJ, Marin GB, Schouten JC (2001) Design of adiabatic fixed-bed reactors for the partial oxidation of methane to synthesis gas. Application to production of methanol and hydrogen-for-fuel-cells. Chem Eng Sci 56(16):4849–4861